Predicting therapeutic windows for synaptic intervention in ALS

Beck Strohmer[1*], Roser Montañana-Rosell[2], Santiago Mora[3], Jessica Ausborn[4†], Ilary Allodi[1,3*†]

[1*]Department of Neuroscience, University of Copenhagen, Blegdamsvej 3B, Copenhagen, 2200, Denmark.
[2]Instituto de Neurociencias, Consejo Superior de Investigaciones Científicas, Universidad Miguel Hernández, Av. Santiago Ramón y Cajal s/n, San Juan de Alicante, 03550, Spain.
[3]School of Psychology and Neuroscience, University of St Andrews, St Mary's Quad, South Street, St Andrews, KY16 9JP, UK.
[4]Department of Neurobiology & Anatomy, Drexel University College of Medicine, 2900 W. Queen Lane, Philadelphia, 19129, PA, USA.

*Corresponding author(s). E-mail(s): beck.strohmer@sund.ku.dk; ia51@st-andrews.ac.uk;
Contributing authors: rmontanana@umh.es; smp27@st-andrews.ac.uk; ja696@drexel.edu;
†These authors contributed equally to this work.

Abstract

Amyotrophic Lateral Sclerosis (ALS) is a fatal and increasingly prevalent disease. We previously identified spinal network changes that contribute to ALS, including a loss of connectivity between spinal V1 inhibitory interneurons and motoneurons. Experimentally stabilizing this connectivity slows disease progression, but the dynamics of network degeneration and optimal time windows for intervention remain elusive. Using a data-driven spiking model with stage-specific degeneration and dynamic synaptic kinetics, we predict that V1 dysregulation induces hyperexcitation and flexor-biased motoneuron activity, disrupting flexor-extensor coordination, potentially contributing to selective vulnerability of flexor motoneurons. Synaptic stabilization that strengthens remaining inhibitory synapses can rescue motor output features even after loss of motoneurons. However, after sustained synaptic loss and the development of slower synaptic dynamics, synaptic

stabilization leads to maladaptive extensor-biased activity, suggesting that excitatory/inhibitory balance impacts treatment effectiveness. Our models inform preclinical strategies by predicting the most effective time window for spinal circuit interventions.

Keywords: neurodegenerative disease, amyotrophic lateral sclerosis, computational modeling, spiking neural network, central pattern generator

1 Main

Amyotrophic Lateral Sclerosis (ALS) is a debilitating disease characterized by progressive motoneuron death with fatal consequences [1, 2]. The exact mechanisms causing motoneuron degeneration in ALS remain elusive, and there is no known cure. ALS features progressive motor dysfunction and synaptic loss [2–5], implicating spinal circuits known as central pattern generators (CPGs), which control motor functions, in disease progression. CPGs drive rhythmic movements, such as walking, breathing, and swallowing [6–9], and locomotor CPGs are affected first in spinal onset ALS [3, 4].

Ventral interneuron classes play a central role in locomotor pattern generation. Inhibitory V1, V2b and V0d, and excitatory V0v, V0c, V0g, V2a and V3 populations are found, among others, in the core of CPGs [8, 9]. V1 populations include Ia interneurons that provide reciprocal inhibition to antagonistic motor pools, Renshaw cells (RCs) that provide recurrent inhibition to motoneurons, and other V1 interneurons with diverse functions, including a population we refer to as $V1_{RG}$ that affects locomotor frequency and contributes to flexor-extensor alternation together with V2b interneurons [10–12].

Despite advances in identifying CPG neuronal subtypes, their synaptic connectivity remains incompletely understood [13]. While *in vivo* and *ex vivo* studies have illuminated the roles of individual populations in locomotion, probing their activity while simultaneously assessing ALS-related degenerative dynamics, remains challenging [4].

To address these issues, we developed the first computational model of ALS disease progression in spinal microcircuits, linking cell-type specific dysregulation to motor output and intervention efficacy. We implemented the spinal locomotor CPG for flexor-extensor alternation as a spiking neural network, incorporating relevant interneuron and motoneuron populations (MNPs). Motor phenotypes from healthy and SOD1G93A ALS mouse models were used to validate network connectivity and subsequent dysregulation [3].

Motoneurons and V1, V0c, and V2a interneurons undergo dysregulation and/or connectivity changes at different stages of ALS progression [3, 4, 14]. V1 synaptic projections are lost early, followed by the loss of V1-specific markers (e.g., Engrailed 1 transcription factor) and V1 cell death, ending later with motoneuron and V2a interneuron loss [3, 4]. In contrast, V0c interneurons respond to network degeneration by temporarily increasing the size of their projecting synapses [14–17].

At the behavioral level, this pattern of dysregulation results in a decrease in locomotor speed and stride length, and hindlimb hyperflexion during early locomotor

phenotypes in the SOD1G93A ALS mouse model [3, 5] (Fig.1a). Hindlimb hyperflexion has been repeatedly linked to V1 interneuron loss in mouse models [11, 18]. Furthermore, differences in flexor and extensor muscle degeneration rate have been observed in patients [19]. Thus opening the question if motoneurons controlling flexor and extensor muscles are affected at similar rates.

Stabilizing V1 synaptic projections using the Extended Synaptotagmin 1 presynaptic organizer improves motoneuron survival and motor output in ALS models [5]. These findings suggest therapeutic potential, but the optimal time window and balance between excitation (E) and inhibition (I) for intervention, remain elusive—questions we address here using computational modeling.

1.1 Results and Discussion

We compared outputs of progressively degenerating spinal networks using computational models to recapitulate motor phenotypes observed in healthy and SOD1G93A mice (Fig.1a-b,g-i). Healthy output was assessed in both the isolated rhythm generator (RG) populations (Fig. 1c) and the flexor and extensor Motoneuron Population (MNP) activity of the full network (Fig.1 d).

A tonic excitatory drive to the RG populations was tuned to reproduce physiologically realistic oscillation frequencies of 2-3Hz (Fig.1d, n, Table B1) and similar firing rates in the flexor and extensor MNPs (Fig.1m, Tables B1, B4). The healthy network model also generated alternating flexor-extensor output (Fig.1p, Table B1) with an extensor-dominated step cycle (Fig.1o, Tables B1, B5), recapitulating previous modeling and experimental observations [20]. An extensor- (flexor-) dominated step cycle is defined by longer extensor (flexor) MNP bursts. We distinguish this from extensor- (flexor-) biased activity, where one MNP fires more strongly than the other.

After validation of healthy network outputs, disease progression was introduced according to previously described network changes in SOD1G93A mice: early loss of V1 synaptic projections at postnatal day (P) 45 (Fig1g, [3]), dysregulation of V1 populations at P63 (Fig1h, [3], [4]) which is further exacerbated at P112 together with dysregulation of motoneurons and V2a interneurons (Fig. 1i, [4]). These stages were implemented by removing cells and connections in proportions derived from experimental data (Fig.1e) [4].

Sample traces show changes in flexor-extensor outputs across disease stages, resulting from the introduced degenerative changes (Fig.1j,k,l). Flexor motoneuron firing rates increased at P45 and P63, indicating a shift towards hyperexcitation (Fig.1m, Fig.2f, h, Table B1), followed by reduced firing rates at P112 (Fig.1m, Fig.2j, Table B1). Flexor-biased activity was observed across all disease time points (Fig.1m, Tables B1, B5). Moreover, output frequency gradually increased (Fig.1n, Table B1), while step cycle transitioned from extensor-dominated at P45 to flexor-dominated at P63 and P112 (Fig.1o, Table B1, B5). Finally, flexor-extensor phase difference decreased with disease progression (Fig.1p, Table B1). Together, these results confirm that the models reproduce key functional signatures of spinal circuit dysregulation in ALS.

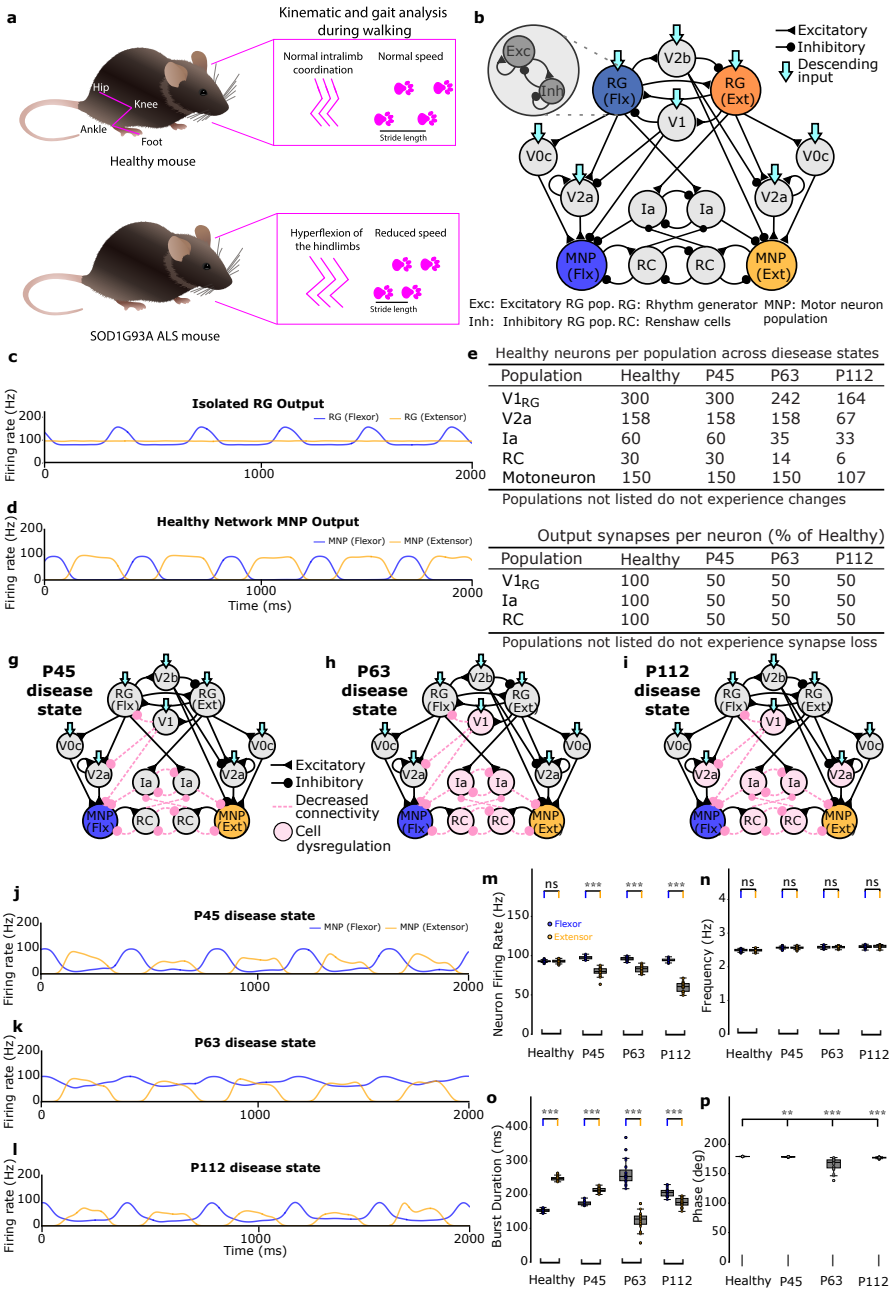

Fig. 1: Computational models of the locomotor CPG in health and during ALS degeneration. a. Early motor phenotype changes observed in the SOD1G93A mouse model. **b**. Connectivity diagram of the healthy network model. **c**. Healthy output of the isolated rhythm-generating populations reflecting the flexor-driven architecture [20] with the flexor in bursting and the extensor in tonic mode. **d**. Healthy MNP output of the complete network showing alternating flexor-extensor activity with an extensor-dominated step cycle. **e**. Number of neurons modeled per time point, replicating biological ratios [4]. **f**. Percentage of synaptic input loss per V1 subpopulation and disease state. **g-i**. Connectivity diagrams of the network without intervention showing synaptic and cell dysregulation across disease stages. **j-l**. MNP output at each time point without intervention. **m-p**. Variance plots comparing flexor versus extensor activity showing flexor-biased activity across disease time points **(m)**, similar flexor-extensor frequency within time points **(n)**, an extensor-dominated step cycle in early disease **(o)**, and degrading phase **(p)**. Variance plots indicate the 50% median line with box edges representing the first and third quartiles, and whiskers at 1.5 times the interquartile range. Significance across conditions was assessed using a Kruskal-Wallis H-test with Dunn's test post hoc **(p)**. Significance comparing flexor versus extensor was assessed using a Wilcoxon Signed-Rank test, n=25; p <= 0.001 = ***, 0.001 > p <= 0.01 = **, 0.01 > p <= 0.05: *, p > 0.05 = 'ns'.

We next simulated synaptic stabilization as a therapeutic strategy to counteract network dysregulation. In the ALS mouse model, synaptic stabilization was administered early during disease progression (P45), preceding motoneuron degeneration and exacerbation of network alterations [5]. Here, we examined the optimal timing of intervention by strengthening remaining V1 synaptic connections in the model (Fig. 2a-d).

After exogenous intervention via synaptic stabilization, we found a reduction in flexor firing rate and flexor-biased activity at all disease time points (Fig.2e, f, g, h, i, j, Tables B2, B5). Furthermore, frequency decreased toward healthy levels across all time points (Fig. 2f, h, j, Table B2). Phase was also rescued at all time points (Fig. 2f, h, j, Table B2). Together, this points to synaptic stabilization of V1 projections as an effective mechanism to ameliorate hyperexcitation of flexor motoneurons during the initial stages of V1 dysregulation.

We also investigated synaptic stabilization at P112 with spared V2a and motoneurons. This again showed a reduction in flexor-biased activity with no changes in phase and frequency compared to healthy controls (Fig. 2k, l, Tables B2, B5). Together, these data suggest that synaptic stabilization of V1 synapses may restore network output despite significant V1 cell dysregulation and synaptic loss.

To predict a therapeutic time window, we investigated additional potential restrictions to the timing of synaptic intervention. In SOD1G93A mice, inhibitory synapses from RCs to motoneurons and excitatory synapses from motoneurons to RCs exhibit slower rise and decay times until P48, when endogenous homeostatic compensation restores synaptic dynamics [21]. We added these slower synaptic dynamics in our P45 model to the inhibitory connections from RCs and Ias to MNPs and to the excitatory connections from MNPs to RCs to test their effects after loss of V1 synaptic connections (Fig. 2m, n).

In the untreated condition, slower synaptic dynamics did not improve flexor-biased activity with increased frequency and decreased phase difference (Fig. 2o-p, Tables B2, B5). When exogenous synaptic stabilization was applied under these conditions, frequency and phase were restored to healthy levels, but induced a shift to extensor-biased activity (Fig. 2q, r, Tables B2, B5). These results suggest that synaptic stabilization in the animal model should be delayed until synaptic dynamics have recovered.

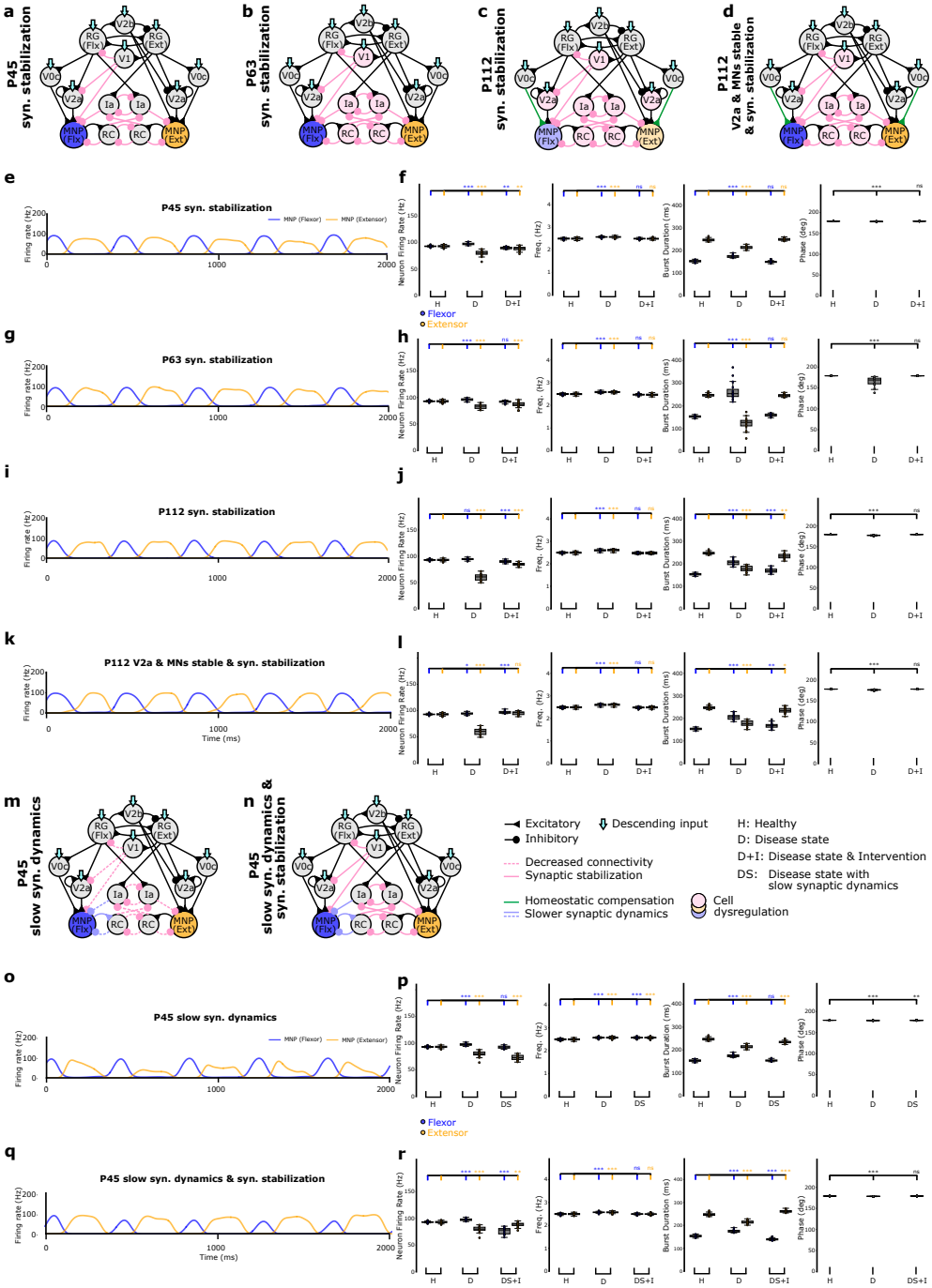

Fig. 2: **Computational models of the locomotor CPG after synaptic stabilization during ALS degeneration. a-d,m,n**. Connectivity diagrams showing network changes and interventions **e,g,i,k,o,q**. Example outputs of flexor and extensor motoneuron populations **f,h,j,l,p,r**. Variance plots comparing healthy, disease, and intervention conditions at different diseases states. Synaptic stabilization reduces flexor-biased activity and restores frequency and phase **(f,h,l)**. Synaptic stabilization promotes extensor-biased activity when applied during slow synaptic dynamics and after synaptic loss **(r)**. Variance plots indicate the 50% median line with box edges representing the first and third quartiles, and whiskers at 1.5 times the interquartile range. Significance across conditions was assessed using a Kruskal-Wallis H-test with Dunn's test post hoc, N=25; p <= 0.001 = ***, 0.001 > p <= 0.01 = **, 0.01 > p <= 0.05: *, p > 0.05 = 'ns'.

Lastly, we investigated V1 rescue in the presence of V2a and motoneuron loss (Fig. B1a). Our model predicted a reduction in flexor-biased activity and restored output frequency and phase difference (Fig.B1b, c, Table B3), indicating that sparing V1 cells and synapses is effective in promoting healthy output.

Overall, the models suggest a threshold in the excitatory/inhibitory balance in the network beyond which exogenous synaptic stabilization may negatively effect motoneuron firing. If stabilization is applied before the synaptic dynamics recover, stabilization can cause maladaptive extensor-biased activity. In the model, slower synaptic dynamics, could only successfully be implemented between the flexor MNP and RCs, since applying them to only the extensor (Fig. B2a), or both (Fig. B2b), increased flexor-biased activity (Fig. B2c, d, e, f, Table B4). This predicts that early synaptic changes may preferentially affect flexor motoneurons, consistent with recent clinical findings of greater flexor muscle involvement in early-stage ALS [19]. Together, our results predict that the time window for effective synaptic intervention precedes substantial motoneuron loss, but only after slow synaptic dynamics are resolved. Furthermore, we suggest that asymmetric cell loss in motoneuron pools should be further investigated.

2 Methods

2.1 Neuron Model

This study uses an adaptive exponential integrate and fire (AdEx) neuron model to maintain computational efficiency while being able to produce both tonic and bursting firing behaviors. The membrane potential V_m for the neuron at each time step (0.1ms) is calculated according to Equations (1) and (2).

$$C\frac{dV_m}{dt} = -g_L(V_m - E_L) + g_L(\Delta T)e^{\frac{V_m - V_{th}}{\Delta T}} - g_e(t)(V_m - E_e) - g_i(t)(V_m - E_i) - w + I_{bias}, \tag{1}$$

$$\tau_w \frac{dw}{dt} = a(V_m - E_L) - w. \tag{2}$$

Reset equation:

$$\text{If } V_m > 0mV, \text{ then } \begin{cases} V_m \to V_{reset} \\ w \to w + b, \end{cases} \text{ and wait } t_{ref}, \tag{3}$$

where V_{th} is the adaptive spike initiation threshold, t_{ref} the refractory period, C the membrane capacitance, I_{bias} the bias current, V_m the membrane potential, g_L the leak conductance, E_L the resting potential, Δ_T the sharpness factor, τ_w the adaptation, a the sub-threshold adaptation conductance, b the spike-triggered adaptation, and V_{reset} the reset potential [22].

In the NEural Simulation Tool (NEST) [23], synaptic conductances are calculated and added directly to the calculation of the membrane potential. The excitatory synaptic conductance is represented by $g_e(t)$, the excitatory reversal potential by E_e, the

inhibitory conductance by $g_i(t)$, and the inhibitory reversal potential by E_i. Gaussian white noise is added to the bias current of individual neurons at each time step. The mean is 0pA and standard deviation is equal to the current bias provided to that neuron. Noise can be negative (inhibitory) or positive (excitatory). The exact values for constants can be found in Table A2 in the Supplementary Material. The parameters are tuned to produce the desired firing behavior as well as a biologically plausible interspike frequency. During in vivo walking, the majority of spinal neurons, including fast motor neurons, are firing in a range of 50-100Hz [24, 25].

As rise and decay times of excitatory post-synaptic currents (EPSCs) and inhibitory post-synaptic currents (IPSCs) are affected during disease progression [21], we implemented a synaptic model where both of these time constants can be manipulated (visualization in Fig. B3 in the Supplementary Material). We use NESTML [26] to create a version of the 'aeif_cond_alpha' neuron model, substituting a beta function to control synaptic conductance. The excitatory and inhibitory dynamics of the beta function are shown in Equations 4.

$$\begin{aligned} g_e(t) &= W_e \left(\frac{1}{\tau_{syn_rise_ex}} - \frac{1}{\tau_{syn_decay_ex}} \right), \\ g_i(t) &= W_i \left(\frac{1}{\tau_{syn_rise_in}} - \frac{1}{\tau_{syn_decay_in}} \right), \end{aligned} \tag{4}$$

where W_e represents the excitatory weight, $\tau_{syn_rise_ex}$ the excitatory rise time constant, $\tau_{syn_decay_ex}$ the excitatory decay time constant, W_i the inhibitory weight, $\tau_{syn_rise_in}$ the inhibitory rise time constant, and $\tau_{syn_decay_in}$ the inhibitory decay time constant. The function is normalized so that if the weight is 1.0, the largest conductance will be 1nS. The synaptic weights are initialized as a distribution using a set mean and standard deviation depending on which populations are being connected. The strength of these connections are manually tuned based on network output and relevant synaptic weights are manipulated during disease progression as described in the Results section. Exact values for the synaptic weights can be found in the source code, available on GitHub [27].

2.2 Healthy Network

The computational model implemented in this study represents the flexor-extensor central pattern generator (CPG) of one side of the lumbar spinal cord [13, 20, 28–32] to produce the antagonistic output controlling flexor-extensor phases of a single limb. Our model implements two rhythm-generating (RG) populations in a half-center oscillator architecture [6, 7], where the RGs mutually inhibit each other through two inhibitory interneuron populations [20, 28, 31, 32]. Each RG comprises both excitatory and inhibitory neurons at a ratio of 4:1. Balance is manipulated through excitatory vs inhibitory synapse strength [33]. Furthermore, excitatory and inhibitory populations contain both bursting and tonically firing neurons [34]. The excitatory neurons in the RGs approximate the Shox2 non-V2a, Hb9, and Lhx9 neurons, which have been

linked to rhythm generation [12, 35]. Shox2 non-V2a have been shown to preferentially contact flexor motoneurons [36]. The number of neurons per population is described in Table A1 in the Supplementary Material. The connectivity details including weights and percentage of connectivity between populations can be found in the source code on GitHub (set_network_params.py) [27].

The bursting neurons contribute to the generation of oscillatory activity in the RG population when receiving a tonic drive. In our study, we assessed network output with two different tonic drives that are applied to each neuron depending on their intrinsic dynamics. The input drive was provided to all neurons in populations indicated by descending input or muscle activity in Fig. 1b. We provided a mean input current to each population, values shown in Table A1, with a standard deviation of 25% of the mean for each. A separate drive was used to excite the Ia neuron populations to induce tonic firing. The flexor RG produced rhythmic activity when isolated from the network, while the extensor RG fired tonically when isolated (see Fig. 1c), following the state-dependent flexor-driven model for rhythm-generation [20, 29, 30, 34]. To produce oscillations in the RG flexor population, 30% of neurons were set to bursting, while the RG extensor included 10% bursting neurons to ensure tonic population activity.

We assert that the inhibitory populations connecting the RGs are equivalent to the $V1_{RG}$ and V2b inhibitory populations which are responsible for intralimb coordination [12] and are known to affect flexor/extensor alternation [3, 11]. Downstream of the RGs, we included the interneuron populations known to be affected in the SOD1G93A ALS mouse model [4, 5, 14], this included the excitatory interneuron populations V2a and V0c as well as the V1 inhibitory interneuron populations Ia and RC. Finally, motoneurons were implemented and acted as the output of the network. The number of neurons and firing behavior per population type is shown in Table A1 in the Supplementary Material.

2.3 Degenerating Network

The network was validated at three progressive time points corresponding to the time points where the transcriptomic data from the SOD1G93A mouse model provided information about degenerated cells [4]. The number of remaining healthy cells across time points for each of the affected populations is outlined in Fig. 1e. Furthermore, all projections from V1 populations - $V1_{RG}$, Ia, and RC were reduced by 50% from postnatal day 45 (P45) and onwards [3] (Fig. 1f). This was implemented through the percentage of connectivity which describes the percentage chance of pre-synaptic neuron connecting to any post-synaptic partner. For example, the V1 subpopulations outside the RG layer projected at a rate of 28% to their post-synaptic partners in the healthy network, from P45 onwards, this is reduced to 14%.

2.4 Testing

The presented results show the variation across 25 trials. The same set of 25 seeds was used for each so that results are comparable. There were several metrics selected to compare network output, these were average maximum neuron firing rate, frequency, phase difference, and burst duration. The neuron firing rate plots are created

by convolving individual spikes with a gaussian window of 20ms. The highest peak was compared to the highest instantaneous firing rate for the population and then the convolved activity was adjusted to ensure the correct firing rate was recorded. The average maximum neuron firing was then calculated by averaging the maximum peak heights of the convolved plot per population within each trial. Frequency was calculated using Equations 5 and 6.

$$period = \frac{\sum(peak2_{mnp} - peak1_{mnp})}{\#_data_points}, \tag{5}$$

$$freq = \frac{1}{period}, \tag{6}$$

where $period$ is the average period of either the flexor or extensor MNP over the simulation, $freq$ is the average frequency of either the flexor or extensor MNP over the simulation, avg_period is the average period of both MNP signals over the simulation. The period and frequency of the signals were calculated using the peaks of the signals, $peak2_{mnp}$ and $peak1_{mnp}$. When calculating using 'findpeaks', the minimum peak height was set to 40% of the maximum amplitude of the signal, the minimum distance between peaks was set to 1000ms, and prominence was set to 0.1. Burst duration was calculated by recording when the population outputs crossed each other and subtracting the time between, the duration for the flexor and extensor MNPs were recorded separately. All of the burst durations over a single trial for the flexor and extensor were then averaged respectively. Phase was determined by calculating the midpoint between the crossings for the flexor and extensor MNPs, as shown in Equation 7.

$$phase_diff = 360 * \frac{midpoint1_{mnp2} - midpoint1_{mnp1}}{midpoint2_{mnp1} - midpoint1_{mnp1}}, \tag{7}$$

$$\text{If } phase_diff > 180, \text{ then } 360 - phase_diff$$

where $phase_diff$ is the phase difference between flexor and extensor MNP output, $midpoint1_{mnp2}$ is the midpoint of the current extensor burst, $midpoint1_{mnp1}$ is the midpoint of the current flexor burst, and $midpoint2_{mnp1}$ is the midpoint of the next flexor burst.

We used two statistical tests to compare the results depending on whether there were two or more conditions to compare. In all experiments, we tested 25 trials per condition and we excluded outlier trials that were outside 3 standard deviations. We applied the non-parametric Kruskal-Wallis H-test with Dunn's test post hoc when comparing experiments. All disease time points were compared to the healthy control. When we compared flexor versus extensor, we applied a Wilcoxon Signed-Rank test. Our significance levels were defined as: p <= 0.001 = ***, 0.001 > p <= 0.01 = **, 0.01 > p <= 0.05: *, p > 0.05 = 'ns'.

Declarations

Funding

This work was funded by the Lundbeck Foundation, Grant no. R426-2023-158 (IA, BS) and Aage og Johanne Louis-Hansens Fond, Grant no. 23-2B-14112 (IA, BS), the School of Psychology and Neuroscience at University of St Andrews (IA), the MRC UKRI, Grant no. MR/Y014901/1 (IA) and the National Science Foundation NSF CRCNS/DARE Grant no. 2113069 (JA).

Competing interests

The authors declare that there are no competing interests.

Ethics approval and consent to participate

Not applicable

Consent for publication

All authors approved the submitted version of the manuscript and consented to publication.

Data availability

All data that support the findings of this study are included within the article and supplementary material. Data sets can be reproduced using the publicly available code.

Materials availability

Not applicable

Code availability

Code used to perform this study is publicly available on GitHub (https://github.com/Allodi-Lab/cpg_modeling_als/) [27].

Author Contributions

BS and IA developed the main idea of the paper. BS researched the biological neural network concepts and implemented the computational model with support from JA. RMR and SM provided data for the paper and commented on the manuscript. The manuscript was written by BS with support from JA and IA. JA and BS created the figure panels for the paper. JA and IA provided theoretical and experimental neuroscientific knowledge and contributed equally as senior authors.

Acknowledgments

The authors would like to thank Associate Professor Alexander Matthias Walter for his input regarding synaptic dynamics. Additionally, we would like to thank Professor Ole Kiehn for his valuable input during the revision process. Finally, we would like to thank Dr. Filipe Nascimento for his insights into synaptic changes during ALS progression.

References

[1] Fogarty, M. J. Amyotrophic lateral sclerosis as a synaptopathy. *Neural regeneration research* **14**, 189–192 (2019).

[2] Mora, S. & Allodi, I. Neural circuit and synaptic dysfunctions in als-ftd pathology. *Frontiers in Neural Circuits* **17** (2023).

[3] Allodi, I., Montañana-Rosell, R., Selvan, R., Löw, P. & Kiehn, O. Locomotor deficits in a mouse model of als are paralleled by loss of v1-interneuron connections onto fast motor neurons. *Nature Communications* **12**, 3251 (2021).

[4] Montañana-Rosell, R. *et al.* Spinal inhibitory neurons degenerate before motor neurons and excitatory neurons in a mouse model of als. *Science Advances* **10**, eadk3229 (2024).

[5] Mora, S. *et al.* Stabilization of v1 interneuron-motor neuron connectivity ameliorates motor phenotype in a mouse model of als. *Nature Communications* **15**, 4867 (2024).

[6] Graham Brown, T. The intrinsic factors in the act of progression in the mammal. *Proceedings of the Royal Society of London. Series B, containing papers of a biological character* **84**, 308–319 (1911).

[7] Graham Brown, T. On the nature of the fundamental activity of the nervous centres; together with an analysis of the conditioning of rhythmic activity in progression, and a theory of the evolution of function in the nervous system. *The Journal of physiology* **48**, 18 (1914).

[8] Kiehn, O. Decoding the organization of spinal circuits that control locomotion. *Nature Reviews Neuroscience* **17**, 224–238 (2016).

[9] Grillner, S. & Kozlov, A. The cpgs for limbed locomotion–facts and fiction. *International Journal of Molecular Sciences* **22**, 5882 (2021).

[10] Gosgnach, S. *et al.* V1 spinal neurons regulate the speed of vertebrate locomotor outputs. *Nature* **440**, 215–219 (2006).

[11] Zhang, J. *et al.* V1 and v2b interneurons secure the alternating flexor-extensor motor activity mice require for limbed locomotion. *Neuron* **82**, 138–150 (2014).

[12] Dougherty, K. J. Distinguishing subtypes of spinal locomotor neurons to inform circuit function and dysfunction. *Current Opinion in Neurobiology* **82**, 102763 (2023).

[13] Rancic, V. & Gosgnach, S. Recent insights into the rhythmogenic core of the locomotor cpg. *International Journal of Molecular Sciences* **22**, 1394 (2021).

[14] Salamatina, A. *et al.* Differential loss of spinal interneurons in a mouse model of als. *Neuroscience* **450**, 81–95 (2020).

[15] Pullen, A. & Athanasiou, D. Increase in presynaptic territory of c-terminals on lumbar motoneurons of g93a sod1 mice during disease progression. *European Journal of Neuroscience* **29**, 551–561 (2009).

[16] Herron, L. R. & Miles, G. B. Gender-specific perturbations in modulatory inputs to motoneurons in a mouse model of amyotrophic lateral sclerosis. *Neuroscience* **226**, 313–323 (2012).

[17] Bak, A. N. *et al.* Cytoplasmic tdp-43 accumulation drives changes in c-bouton number and size in a mouse model of sporadic amyotrophic lateral sclerosis. *Molecular and Cellular Neuroscience* **125**, 103840 (2023).

[18] Britz, O. *et al.* A genetically defined asymmetry underlies the inhibitory control of flexor–extensor locomotor movements. *Elife* **4**, e04718 (2015).

[19] Milella, G. *et al.* Mapping lower-limbs muscle vulnerability in patients with als: The role of upper and lower motor neurons. *Journal of the Neurological Sciences* **462**, 123098 (2024).

[20] Shevtsova, N. A. *et al.* Organization of left–right coordination of neuronal activity in the mammalian spinal cord: Insights from computational modelling. *The Journal of physiology* **593**, 2403–2426 (2015).

[21] Nascimento, F. *et al.* Spinal microcircuits go through multiphasic homeostatic compensations in a mouse model of motoneuron degeneration. *Cell reports* **43** (2024).

[22] Naud, R., Marcille, N., Clopath, C. & Gerstner, W. Firing patterns in the adaptive exponential integrate-and-fire model. *Biological cybernetics* **99**, 335 (2008).

[23] Valverde, J. A. E. *et al.* Nest 3.7 (2024). URL https://doi.org/10.5281/zenodo.10834751.

[24] Wu, Y. *et al.* Ultraflexible electrodes for recording neural activity in the mouse spinal cord during motor behavior. *Cell reports* **43** (2024).

[25] Jensen, D. B., Kadlecova, M., Allodi, I. & Meehan, C. F. Spinal motoneurones are intrinsically more responsive in the adult g93a sod1 mouse model of amyotrophic lateral sclerosis. *The Journal of physiology* **598**, 4385–4403 (2020).

[26] Linssen, C. A. *et al.* Nestml 7.0.0. doi:10.5281/zenodo.10125416 (2023).

[27] Strohmer, B. Cpg als model source code (2025). URL https://github.com/Allodi-Lab/cpg_modeling_als. Last accessed on 22. May, 2025.

[28] Kiehn, O. & Dougherty, K. in *Locomotion: circuits and physiology* 1623–1651 (Springer, 2022).

[29] Ausborn, J., Snyder, A. C., Shevtsova, N. A., Rybak, I. A. & Rubin, J. E. State-dependent rhythmogenesis and frequency control in a half-center locomotor cpg. *Journal of neurophysiology* **119**, 96–117 (2018).

[30] Latash, E. M. *et al.* On the organization of the locomotor cpg: insights from split-belt locomotion and mathematical modeling. *Frontiers in Neuroscience* **14**, 598888 (2020).

[31] Rybak, I. A., Dougherty, K. J. & Shevtsova, N. A. Organization of the mammalian locomotor cpg: review of computational model and circuit architectures based on genetically identified spinal interneurons. *ENeuro* **2** (2015).

[32] Ausborn, J., Shevtsova, N. A. & Danner, S. M. Computational modeling of spinal locomotor circuitry in the age of molecular genetics. *International Journal of Molecular Sciences* **22**, 6835 (2021).

[33] Strohmer, B., Najarro, E., Ausborn, J., Berg, R. W. & Tolu, S. Sparse firing in a hybrid central pattern generator for spinal motor circuits. *Neural computation* **36**, 759–780 (2024).

[34] Hägglund, M. *et al.* Optogenetic dissection reveals multiple rhythmogenic modules underlying locomotion. *Proceedings of the National Academy of Sciences* **110**, 11589–11594 (2013).

[35] Bertho, M. *et al.* Excitatory spinal lhx9-derived interneurons modulate locomotor frequency in mice. *Journal of Neuroscience* **44** (2024).

[36] Dougherty, K. J. *et al.* Locomotor rhythm generation linked to the output of spinal shox2 excitatory interneurons. *Neuron* **80**, 920–933 (2013).